NASA/TM-2019-220195

THE INTERMEDIATE WAKE OF A THIN FLAT PLATE WITH A CIRCULAR TRAILING EDGE

Man Mohan Rai
Ames Research Center
Moffett Field, CA-94035

April 2019

NASA STI Program ... in Profile

Since its founding, NASA has been dedicated to the advancement of aeronautics and space science. The NASA scientific and technical information (STI) program plays a key part in helping NASA maintain this important role.

The NASA STI program operates under the auspices of the Agency Chief Information Officer. It collects, organizes, provides for archiving, and disseminates NASA's STI. The NASA STI program provides access to the NTRS Registered and its public interface, the NASA Technical Reports Server, thus providing one of the largest collections of aeronautical and space science STI in the world. Results are published in both non-NASA channels and by NASA in the NASA STI Report Series, which includes the following report types:

- TECHNICAL PUBLICATION. Reports of completed research or a major significant phase of research that present the results of NASA Programs and include extensive data or theoretical analysis. Includes compilations of significant scientific and technical data and information deemed to be of continuing reference value. NASA counterpart of peer-reviewed formal professional papers but has less stringent limitations on manuscript length and extent of graphic presentations.

- TECHNICAL MEMORANDUM. Scientific and technical findings that are preliminary or of specialized interest, e.g., quick release reports, working papers, and bibliographies that contain minimal annotation. Does not contain extensive analysis.

- CONTRACTOR REPORT. Scientific and technical findings by NASA-sponsored contractors and grantees.

- CONFERENCE PUBLICATION. Collected papers from scientific and technical conferences, symposia, seminars, or other meetings sponsored or co-sponsored by NASA.

- SPECIAL PUBLICATION. Scientific, technical, or historical information from NASA programs, projects, and missions, often concerned with subjects having substantial public interest.

- TECHNICAL TRANSLATION. English-language translations of foreign scientific and technical material pertinent to NASA's mission.

Specialized services also include organizing and publishing research results, distributing specialized research announcements and feeds, providing information desk and personal search support, and enabling data exchange services.

For more information about the NASA STI program, see the following:

- Access the NASA STI program home page at http://www.sti.nasa.gov

- E-mail your question to help@sti.nasa.gov

- Phone the NASA STI Information Desk at 757-864-9658

- Write to:
  NASA STI Information Desk
  Mail Stop 148
  NASA Langley Research Center
  Hampton, VA 23681-2199

NASA/TM-2019-220195

THE INTERMEDIATE WAKE OF A THIN FLAT PLATE WITH A CIRCULAR TRAILING EDGE

Man Mohan Rai
Ames Research Center
Moffett Field, California

National Aeronautics and
Space Administration

Ames Research Center
Moffett Field, California 94035-1000

April 2019

THE INTERMEDIATE WAKE OF A THIN FLAT PLATE WITH A CIRCULAR TRAILING EDGE

Man Mohan Rai*
NASA Ames Research Center, Moffett Field, CA-94035, USA

ABSTRACT

The intermediate wakes of thin flat plates with circular trailing edges (TEs) are investigated here with direct numerical simulations (DNSs). The separating boundary layers are turbulent in all cases. The near wake in two thin-plate cases (IN & NS), with a focus on the vortex shedding process, was explored in a recent article. Intermittent shedding was observed in Case IN. Case NS, with half the TE diameter of Case IN, was an essentially non-shedding case. A third case (ST) with a sharp trailing edge was also investigated and found to exhibit an intermittent wake instability. The objectives of the present study are twofold. The first is to determine if the wake instability found in Case ST exists in Cases IN and NS as well. The second is to provide the distributions of the turbulent normal intensities and shear stress in the wake and to understand these distributions via the budget terms in the corresponding transport equations. The results show that both Cases IN & NS exhibit a wake instability in the intermediate wake region, that is similar to that found earlier in Case ST. We note that in Case IN, the presence of an intermediate-wake instability results in the co-existence of two different types of instability within a single wake. The distributions of the turbulent normal intensities and shear stress, and the budget terms for the streamwise intensity are included and discussed here. All the budget terms contribute appreciably to the overall budget in the transport equation for streamwise normal intensity.

1. INTRODUCTION

An investigation of the wake of the thick flat plate with a circular trailing edge and turbulent separating boundary layers, was initiated by Rai (2013, 2014 & 2015). This was accomplished with the aid of direct numerical simulations (DNSs). The boundary layers as well as the wake were computed via DNS in these investigations. The separating boundary layers are fully turbulent well upstream of the trailing edge (TE) and are statistically identical in these investigations. The wake is symmetric in the mean and vortex shedding is vigorous in all the cases investigated (Cases A - D). Unlike the case of the cylinder, the Reynolds number based on momentum thickness of the boundary layer just upstream of the TE (Re_θ) and the Reynolds number defined using the thickness of the flat plate or the diameter of its TE (Re_D), are independent parameters. Collectively, the articles by Rai (2013, 2014 & 2015) address several aspects of the flat plate wake such as the instability of the detached shear layers (DSLs), entrainment, the distribution of phase-averaged turbulence intensities and shear stress and associated production terms.

The objective of the more recent investigations by Rai (2017, 2018a) is to understand the changes in the characteristics of the wake of a flat plate with turbulent separating boundary layers (in particular changes in vortex shedding), as the plate becomes thin in *relation* to the boundary layer thickness (increasing θ/D). The TE of the plate *remained circular* in the cases investigated in these two articles. Changes obtained with increasing θ/D, in the coherence of the shed vortices (spanwise direction, z), in the roll-up of the detached shear layers (DSLs) and time-averaged velocity statistics are discussed. The continuity of the shedding process is demonstrated and the appearance of significant variation in shedding

* Senior Researcher, Computational Sciences, Exploration Technology Directorate.

intensity and frequency is noted in these articles. Important contributors to the substantial changes in the observed flow features as θ/D is increased are identified.

The five cases investigated in Rai (2017, 2018a) are labeled Cases A, D, E, F & G. Case A is the reference case (thick plate). Values of Re_D and the ratio $\psi = (\theta/D)/(\theta/D)_{Case\ A}$ for these five cases are provided in Table 1. The ratio ψ is essential in comparing the value of (θ/D) for any given case to that of the reference case (Case A); it varies substantially over the cases considered (by a factor of 51.6). Table 1 also provides the value of ψ for Cases IN & NS, which were computed for the present investigation and for an earlier one (Rai, 2108b). The Reynolds number based on plate length L is the same in all the cases listed in Table 1, $Re_L = 1.25 \times 10^6$.

	Re_D	ψ
Case A	10,000	1.0
Case D	5000	2.3
Case E	2500	4.9
Case F	625	20.4
Case G	250	51.6
Case IN	100	129.0
Case NS	50	258.0

Table 1. The parameters Re_D and ψ for Cases A, D, E, F & G (Rai 2017, 2018a) and IN & NS.

The following is a brief summary of the findings of Rai (2017, 2018a). The DNSs of the flat plate wakes show that vortex shedding is vigorous in the low θ/D cases (Cases A and D) and that there is a substantial decrease in shedding intensity as θ/D increases (Cases E, F & G). Shedding intensity here and elsewhere in the article refers to the strength of the vortex as measured by peak spanwise vorticity magnitude and/or related pressure minimum, or peak upwash/downwash generated near/at the wake centerline. A lack of coherence in the spanwise structure of the shed vortices is observed with increasing θ/D. The interaction between the upper and lower DSLs becomes stronger as θ/D is increased. The proximity of the DSLs in the large θ/D cases essentially reduces their ability to roll-up and contribute to the strength of the newly formed shed vortices. In Case F the shear layers are so close to each other that the roll-up is essentially prevented and the shed vortices form and remain within the shear layer in the near wake. Case G is similar to Case F in these respects.

An initial examination of shedding in Case F via contours of cross-stream velocity at the wake center-plane ((t, z) plane) at a given x location and also the method of Jeong & Hussain (1985, λ_2 criterion) indicated that vortex shedding may be intermittent. Quiescent regions, between regions of shedding activity, both in time and in the spanwise direction were observed. These regions are an indication of potential intermittency in the shedding process. However, a closer look at the shedding process, using fluctuations in TE surface vorticity and animations of velocity vectors, showed that vortex shedding is continuous in time although strengthened/weakened during certain periods in Cases F & G. The investigation showed that boundary layer disturbances (streamwise vortices) can increase/decrease vortex shedding intensity. This effect of streamwise vortices on the shed vortices also has implications with regard to shed vortex structure. The shed vortices are enhanced/weakened over the short distances in the z direction over which the influence of the streamwise vortices is felt. Thus, this phenomenon is at the same time also a contributor to the loss of spanwise coherence of the shed vortices.

The role of boundary layer velocity fluctuations near the TE as a causative agent of large fluctuations in shedding period was examined; it was found that high- and low-speed streaks cause decreases/increases in shedding period, respectively. This also implies that these streaks affect shed vortex structure; increases/decreases in shedding frequency are obtained over a z-extent that corresponds

to the characteristic widths of these streaks, thus contributing to the loss of spanwise coherence of the shed vortices. The effect of increasing the ratio θ/D on centerline velocity spectra and time-averaged wake velocity statistics is also discussed in the two articles.

In Rai (2018b) the TE thickness is reduced to values considerably below that of Case G, and all the way to a sharp TE. The wake of the thin flat plate with a sharp TE and turbulent boundary layers has been discussed in several articles, one of the earliest being that of Chevray & Kovasznay (1969). The ratio of the boundary layer momentum thickness to the TE thickness of the plate (θ/D) is large (23.2) in their study. Profiles of measured mean velocity and turbulent normal intensities and shear stress in the wake are provided. The boundary layers merge gradually to form the wake. Large-scale vortex shedding is absent. Other notable experimental investigations of the thin flat plate with a sharp trailing edge include those of Ramaprian et al (1982), Nakayama & Liu (1990), Hayakawa & Iida (1992) and Thomas & Liu (2004). In addition to the experimental investigations mentioned above, analytical solutions based on simplifying assumptions are provided by Alber (1980). In this study the centerline velocity distribution in the streamwise direction (x) in a region of the near wake is approximated by a logarithmic relation similar in form to that obtained for the turbulent boundary layer upstream of the wake in these cases. A good comparison is obtained between experimental data and the 'wake log-law' in the near wake.

The near and very near wake of thin flat plates with both sharp and circular trailing edges are investigated with direct numerical simulations in Rai (2018b). The TE is circular in two of the cases (IN & NS) and sharp in one of them (ST). The separating boundary layers are turbulent in all cases. The focus of this study was to explore the effect of significantly reducing Re_D on the near wake. Case NS, with the lowest value of Re_D computed thus far (with a circular TE), was found to be an essentially non-shedding case; only one shed vortex was observed over a time period corresponding to 20 shedding periods of Case IN. The TE flow exhibited oscillations in the direction of motion (upward/downward) as a result of disturbances in the DSLs (such as vortices and other flow features). The *v* spectrum at x/D = 1.0 did not exhibit a peak despite the oscillating flow direction. Case NS is the flat plate equivalent of the extremely low Reynolds number cylinder cases where attached eddies and vortex shedding are both absent. Case IN, also with a circular trailing edge but twice the value of Re_D as in Case NS, exhibited intermittent shedding. Shedding was initiated when the TE flow direction changed rapidly *due to turbulence*. Calm periods in Case IN resulted in TE flow with two attached eddies much like low Reynolds number cylinder flow. The resulting flow pattern is very similar to that obtained for the computed *mean* flow in Case IN. Unlike Case NS, Case IN shows a shedding related peak in the near-wake, centerline *v* spectrum.

While the focus in Rai (2018b) was the near wake of Cases IN & NS, here we explore the intermediate wake of these two cases. One of the objectives in computing Case ST was to understand the reasons underlying some of the experimental findings of Hayakawa & Iida (1992); that is, peak values in normal intensity and shear stress profiles in the y direction were found to first increase in the x direction, from that obtained at the TE, before decreasing further downstream. In addition, a broadband peak was obtained in centerline cross-stream velocity spectra, indicating quasi-periodicity (possibly due to vortices or wave-like motions). These features were observed in the computation (Case ST) as well. Case ST showed a near wake instability resulting in spanwise vortices near the wake centerline (with at times a streamwise component). The instability is intermittent but occurs frequently and is sufficiently powerful to cause a broadband peak in the *v* spectrum (as in the experiment). The instability related vortices are contributors to the significant increase in near-centerline normal intensity values in Case ST and very likely in the experiment as well.

The presence of the wake instability in Case ST raises the possibility of a similar instability in Cases IN & NS. The intermittent shed vortices in Case IN disappear soon after they are formed and Case NS is an essentially non-shedding case. Hence, there is the distinct possibility that both these cases also exhibit a wake instability of the type seen in Case ST, but further downstream in the intermediate wake. Here we explore the intermediate wake of Cases IN & NS with two objectives in mind; to ascertain the

presence/absence of a wake instability and to understand the distribution of normal intensities and shear stress via the distributions of the budget terms in the corresponding transport equations. The presence of an intermediate-wake instability in Case IN would result in the co-existence of two different types of instability in the wake.

2. FLAT-PLATE COMPUTATIONAL GRID, FLOW/GEOMETRY PARAMETERS AND NUMERICAL METHOD

The computational region for the DNSs of the flat plates with a circular TE is divided into two zones to facilitate grid generation and provide adequate grid resolution for the wake. Figure 1 shows a typical plate cross-section and the two zones that comprise the computational region. The three-dimensional zones and grids are obtained by uniformly spacing copies of these two-dimensional zones in the z direction. The plate zone is bounded by four boundaries: the plate surface (excluding the trailing edge), an external boundary and, two zonal boundaries (top and bottom) that interface with the wake zone. The wake zone is constructed to provide adequate grid resolution for the DSLs, the recirculation region (if any) and the wake. The boundaries of this zone include the circular TE, the upper and lower boundaries and the exit boundary. Both the upper and lower boundaries consist of a zonal boundary segment that interfaces with the plate zone and a second segment that serves as an external boundary. The coordinate system shown in Fig. 1 is only indicative of the coordinate directions; the origin is at the center of the circular TE (as in Fig. 2).

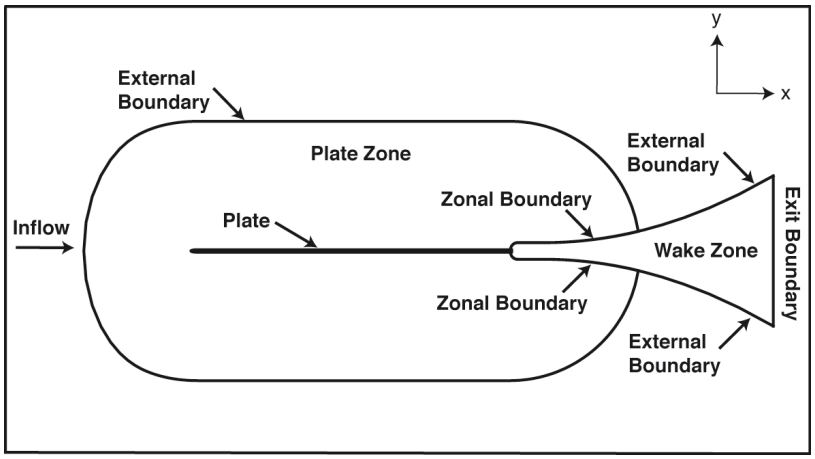

Figure 1. Midspan plate section and multiple zone discretization of the computational region for the circular TE cases (Rai 2013).

The placement of the various boundaries in relation to the plate surface in Cases A & D is provided in Rai (2013, 2014 & 2015). The vertical extent of the wake zone near the TE, where its upper/lower boundaries are horizontal is large enough to completely contain the wake in all cases (Fig. 4 in Rai 2013 clearly shows the adequacy of this dimension in Case A). The spanwise extent of the region in Cases A & D is 4.0D. *Cases A & D are labeled as A & D in Rai (2015) as well.*

Figure 2 shows representative grids in the vicinity of the TE in both zones. Both the grids have the same spacing in the wall normal direction at the plate surface. Downstream of the region of interest ($x/D \approx 13.5$ in Cases A & D and larger x/D values in the other cases), the wake grid coarsens gradually in the x direction. This coarsening reduces computational costs and dissipates the wake to a degree that inviscid exit boundary conditions can be employed at the exit boundary of the wake zone. The wake grid for Case A was constructed with 741 grid points in the streamwise direction, 411 in the cross-stream direction and 256 in the spanwise direction (about 78 x 10^6 grid points). The resolution achieved along the centerline in the three spatial directions at x/D = 10.0 is approximately $\Delta x/\eta = 3.7$, $\Delta y/\eta = 2.2$ and $\Delta z/\eta = 2.1$ where η is

the computed Kolmogorov length scale at the same location. The grid resolution in the plate grid in the x, y and z directions for this case is about 17.8, 0.84 and 6.6 wall units respectively, based on the wall shear velocity near the end of the plate. The grid resolution achieved in cases A, D, E, F & G, is similar. The adequacy of the grid resolution and domain size used is demonstrated in Rai (2013 & 2014). The computations are all performed at the same freestream Mach number of 0.2. Compressibility effects are quite small at this Mach number.

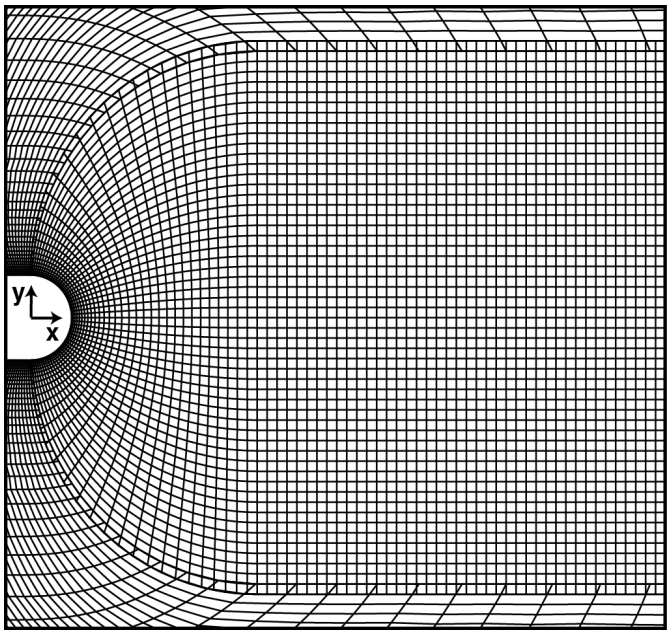

Figure 2. Representative grids in the plate and wake zones in the trailing edge region (Rai 2013).

The primary goal in the current investigation and in Rai (2017 & 2018a) is to study the effect of substantially increasing θ/D on various characteristics of the wake. Accordingly, the thickness of the plate in Cases E, F & G was reduced by a factor of 2, 8 & 20, respectively, from that used in Case D. The length of the plate in Cases E, F & G was the same as in Cases A & D. In Cases E, F & G the extent of the computational region in the z direction (Δz) in terms of this constant plate length (L) was kept the same as in Case D to ensure that the computed statistics on the plate were not affected by the imposition of periodicity in the z direction. However, the thickness of the plate was reduced as mentioned earlier. The grid resolution in the z direction is the same as in Case D. For the same reason (an accurate simulation/representation of the separated boundary layer), the vertical extent of the wake region (in the region where the upper and lower boundaries are horizontal) was also maintained at approximately the same value as in Case D. The same reasoning was also used in the placement of the external boundary of the plate zone and the exit boundary of the wake zone in Cases E, F & G. Values of Re_D and the ratio $\psi = (\theta/D)/(\theta/D)_{Case\ A}$ for Cases A, D, E, F & G were provided in Table 1. The Reynolds number based on plate length L is the same in all cases, $Re_L = 1.25 \times 10^6$.

The computational domains for Cases IN & NS were obtained using the same principles as in Cases E, F & G. The z-extent of the computational domain and the grid resolution used in this direction are the same as in Cases D, E, F and G. However, the grid resolution in the (x, y) plane in the TE region is much finer in order to resolve the geometry and flow in this region. The resolution in the (x, y) plane in the TE region is significantly more than required for the upstream turbulent boundary layer of the plate (less than about 0.25 wall units in the wall-tangential/normal directions in Case IN, and even finer in Case NS).

A high-order accurate upwind-biased method is used here to compute the flow over the plate as well as that in the wake. The convective terms are computed using sixth- and seventh-order upwind-biased finite differences, both with seventh-order dissipation terms. These dissipation terms are the naturally occurring truncation error terms that are obtained in the upwind-biased finite-difference approximation to the convective terms. The viscous terms are computed with fourth-order central differences. The method is iterative-implicit in nature, multiple iterations are employed at each time-step to solve the nonlinear finite-difference equations arising from a fully implicit formulation; the method is second-order accurate in time. The boundaries that contain the computational grids can be classified as natural and zonal boundaries. The natural boundaries include the external boundary of the plate grid, the surface of the plate, the exit boundary of the wake grid, the segments of the upper and lower boundaries of the wake grid labeled as "external boundary" in Fig. 1, and, the boundaries in the *z* direction. The upstream segment of the upper boundary between the plate and wake grids is an example of the zonal boundaries used in the computation. Periodic boundary conditions are imposed on the boundaries in the *z* direction (homogeneity in *z*). No-slip/adiabatic wall conditions are used on the plate surface. Wall blowing/suction is implemented on a short segment on both the upper and lower surfaces of the plate to induce transition to turbulence. The boundary layer is turbulent well upstream of the trailing edge. The upper and lower transitional/turbulent boundary layers and the wake are all computed via DNS. The natural and zonal boundary conditions, and the high-order accurate upwind-biased finite-difference method used here are discussed in detail in the present author's earlier articles cited in Rai (2015).

A discussion of the adequacy of the resolution used in the computations presented here via comparisons of DNS data obtained using the present method with 1) experimental cylinder wake data (Ong, Wallace & Moin, 1995) and 2) boundary layer data (Karlsson & Johansson, 1988) is provided in Rai (2017). An extensive comparison of the DNS data obtained for fully developed turbulent channel flow with an earlier version of the present method (lower-order of spatial accuracy for the inviscid terms, Rai & Moin 1991) and spectral method data (Kim Moin & Moser, 1987) is also discussed in Rai (2017). These comparisons demonstrate the adequacy of the grid resolution used in the plate and wake grids. The adequacy of the size of the computational domain in all three spatial directions is also discussed at length in Rai (2017). In the interest of brevity these discussions have been omitted in the present article.

3. INTERMEDIATE WAKE PHYSICS IN CASES IN & NS

The focus in this section is on the prevalent flow features in the intermediate wake with an emphasis on a possible wake instability. As mentioned earlier, the presence of the wake instability in Case ST raises the possibility of a similar instability in Cases IN & NS. The intermittent regions of circulating flow (TE vortex shedding) in Case IN disappear soon after they are formed (within a few diameters) and Case NS is an essentially non-shedding case. Hence, there is the possibility that both these cases exhibit a wake instability of the type seen in Case ST, but in the intermediate wake. In the following contour plots the colors blue/green represent negative values (deep blue representing the lowest value) of the term/quantity being discussed. Orange, red and magenta represent positive values (magenta bordering on white representing the highest value). Shades of yellow represent values close to zero.

3.1 Case IN

The behavior of the upper and lower DSLs in the intermediate wake region in Case IN is investigated in this sub-section. Figure 3 shows contours of instantaneous spanwise vorticity in a (x, y) plane at three instants in time (different *z* locations). The dominant feature at two of the instants (labelled as Events A & E, Figs. 3a & 3b) is a set of spanwise vortices (for the most part of alternating sign). They are seen within both DSLs as regions of clustered contours with an associated peak, in the range $-9.0 < y/D < 9.0$ for $x/D > 20.0$. Some minor sinuous motion is apparent upstream of $x/D = 20.0$ as well. Further downstream, these nascent vortices evolve into well-developed spanwise vortices. Contours of streamwise

and cross-stream vorticity show that some of them possess streamwise and cross-stream components of vorticity as well. In contrast to the behavior observed in Figs. 3a & 3b, Fig. 3c shows a period in time when the intermediate wake is quiescent (labelled Event F, see rectangle).

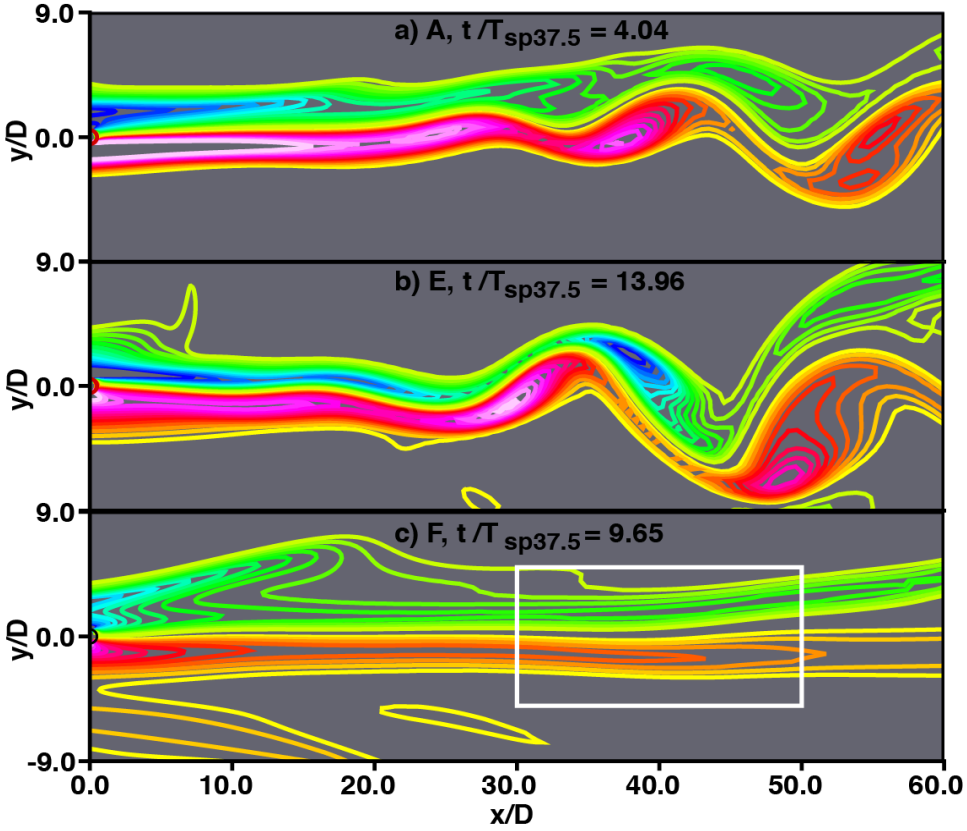

Fig. 3. Contours of instantaneous spanwise vorticity in a (x, y) plane, a) Event A, b) Event E and c) Event F, Case IN.

The question that arises is as follows: Is the wake instability observed in Figs. 3a & 3b a rare phenomenon or does it occur frequently? Figure 4 shows contours of cross-stream velocity (*v*) as a function of time and z (in a (t, z) plane) at x/D = 37.5 (intermediate wake) and y/D = 0.0. Similar plots (utilizing fluctuating pressure, streamwise and cross-stream velocity components were used effectively in Rai (2010, 2015, 2017 & 2018a) to study both shear layer vortices and shed vortices. The passage of shed vortices and shear layer vortices (largely spanwise vortices) past a given point results in alternating bands of opposite sign of the quantity of interest (blue/red, in this case *v*). Such pairs of bands (in some cases multiple pairs) are observed in Fig. 4. The red/blue bands represent upwash/downwash at the wake center-line. Six different regions (events) from Fig. 4 were identified for further study. They are marked with rectangles. Events A, E & F from Fig. 3 are included in this group. The time-scale used to normalize time in Fig. 4 is discussed shortly.

Events B & D also showed an instability of the type seen in Figs. 3a & 3b. Event C, similar to Event F did not exhibit near-centerline spanwise vortices. It is clear from Fig. 4 that the wake instability of Figs. 3a & 3b is not an infrequent occurrence. It is a dominant feature of the intermediate wake in Case IN. The spanwise vortices of Figs. 3a & 3b were confirmed using both the λ_2 criterion of Jeong & Hussain (1995) and instantaneous velocity vectors; circulating flow was evident after subtracting the velocity at the center of the candidate vortex. These two tests were also performed for the vortices of the different events identified in Fig. 4 as periods of instability.

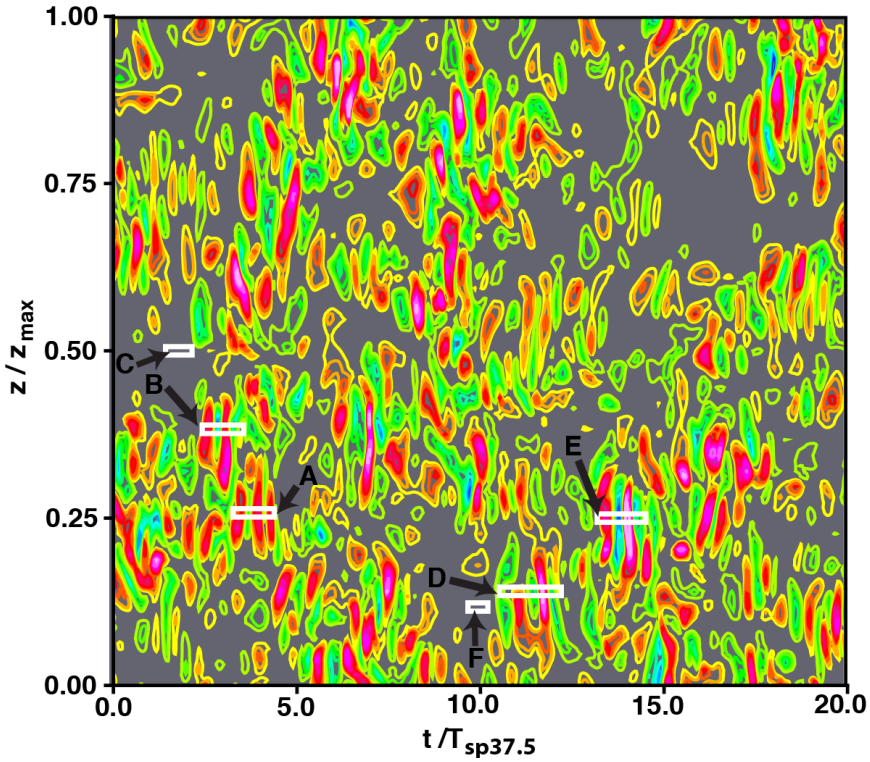

Fig. 4. Contours of *v* in a (t, z) plane at x/D = 37.5, y/D = 0.0, Case IN.

The frequent occurrence of the intermediate-wake instability leads to the expectation of a broadband peak in the spectrum obtained for *v* at the location x/D =37.5, y/D = 0.0. Figure 5 shows this spectrum along with the one obtained in the very near wake at x/D = 1.0. The spectrum at x/D = 1.0 is reproduced from Rai (2018b), Fig. 16 in that article; the peak in this spectrum is caused by the intermittent shedding observed in Case IN. The broadband peak obtained at x/D = 37.5 is evident.

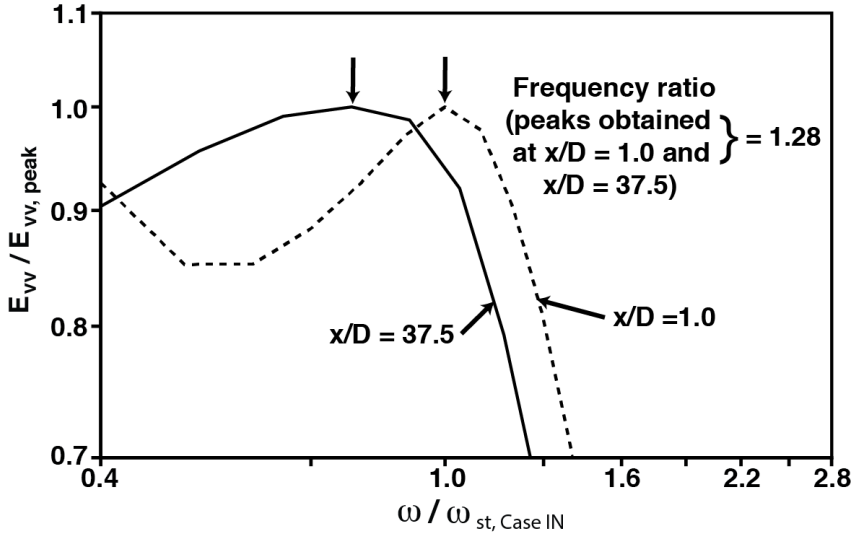

Fig. 5. Comparison of *v* spectra obtained at x/D = 1.0 & 37.5, y/D = 0.0, Case IN.

The one obtained at x/D = 1.0 is considerably sharper. The ratio of frequencies is 1.28 (frequency corresponding to peak at x/D = 1.0 to that at x/D = 37.5); both peaks are identified with arrows. Frequencies are normalized with the peak-related-frequency obtained at x/D = 1.0. The appearance of the intermediate-wake instability in Case IN results in the co-existence of two different types of instability within a single wake. The shedding related instability is not evident past a few diameters downstream of the trailing edge of the plate. Nevertheless, the intermittent shedding (and associated peak-related frequency) may be a contributor to the location (peak-related frequency) of the broadband peak obtained at x/D = 37.5. The time-scale used to normalize time in Figs. 3 & 4 is obtained from this broadband-peak-related frequency.

Of interest are the contributors to the strengthening/weakening of the wake instability. In Rai (2010) the inviscid, incompressible form of the transport equation for spanwise vorticity (Eq. 1 below) was used in investigating the growth of disturbances in the DSLs of a cylinder at low Reynolds number (Re_D = 3900, laminar separation). The vortex stretching & rotation terms, from the full transport equation that includes the viscous terms, have been retained on the RHS of Eq. 1.

$$\frac{D\omega_z}{Dt} = T_1 + T_2 + T_3 \quad ; \quad T_1 = \omega_x \frac{\partial w}{\partial x}; \quad T_2 = \omega_y \frac{\partial w}{\partial y}; \quad T_3 = \omega_z \frac{\partial w}{\partial z} \tag{1}$$

The variables ω_x , ω_y and ω_z are the components of vorticity in the *x*, *y* and *z* directions, respectively, and *w* is the spanwise component of velocity. In Rai (2018a) the instantaneous distribution of the term T_3 in a cross-plane (y, z) at a given x location in the wake was used to explain the strengthening/weakening of shed vortices via the *w* velocity field caused by streamwise vortices in the DSLs.

Here we utilize the terms $T_{i,avg}$, (i = 1, 3), defined as the product of the instantaneous values of the terms T_i (Eq. 1) multiplied by the sign of the instantaneous spanwise vorticity ω_z, averaged over time, at any given spatial location. Time-averaging is performed over specified periods when the wake is unstable or quiescent, for example over the time period corresponding to Event A in Fig. 4. Thus, regions of positive $T_{i,avg}$ contribute to the enhancement of ω_z over the given period (regardless of the sign of ω_z) and regions of negative $T_{i,avg}$ have the opposite effect. The contribution of each of the three terms, T_i, to the evolution of ω_z can thus be determined. Distributions of $T_{i,avg}$ in a cross-plane (y, z) are of particular interest.

Figures 6a - 6d show contours in an end-plane (y, z), at x/D = 37.5, of the terms $T_{1,avg}$, $T_{2,avg}$, $T_{3,avg}$ and the sum $\Sigma = T_{1,avg} + T_{2,avg} + T_{3avg}$, respectively, for Event A. The minimum and maximum values and the number of contours in each sub-plot of Fig. 6 are the same; thus, the magnitude of the contribution of each term to the evolution of the vortices associated with the wake-instability can be directly compared (this is the case in Figs. 7a – 7d as well). The long white rectangle in Figs. 6a – 6d is at the central z location of Event A (see Fig. 4) and its extent in the y direction is representative of the y extent of the instability vortices. Clearly, the term $T_{1,avg}$ does not contribute significantly to the enhancement of the spanwise vorticity associated the wake-instability-vortices. The term $T_{2,avg}$, on the other hand, results in an overall weakening of these vortices during Event A. The term $T_{3,avg}$ contributes significantly to the strengthening of these vortices; it is the dominant term. It dominates the negativity of the term $T_{2,avg}$ to an extent that the distribution of Σ closely resembles that of the term $T_{3,avg}$. This of course results in Event A being a period of well-defined wake instability.

Figures 7a – 7d show contours of Σ in an end-plane (y, z), at x/D = 37.5, for Events B, C, D and E, respectively. As expected (from the bands in Fig. 4), instability Events B, D & E are enhanced by the RHS of Eq. 1, whereas the time-period corresponding to Event C shows Σ having a calming effect on any potential instability. As in Event C, the distribution of Σ obtained in Event F is not instability enhancing. The term $T_{1,avg}$ only provided a minor contribution in Events A – F.

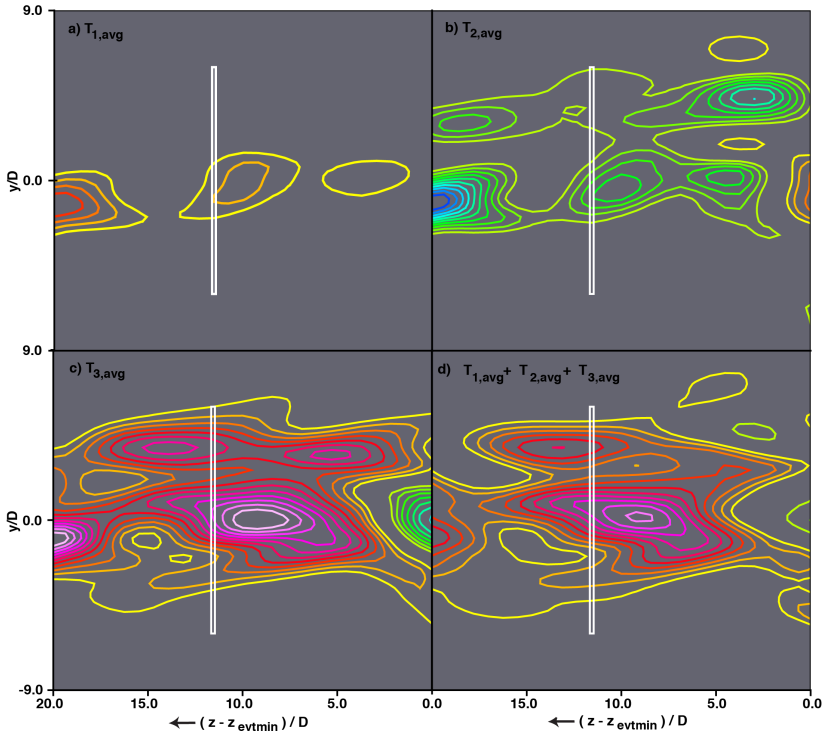

Fig. 6. Contours in an end-plane (y, z) at x/D = 37.5 of a) $T_{1,avg}$, b) $T_{2,avg}$, c) $T_{3,avg}$, and d) Σ, Event A, Case IN.

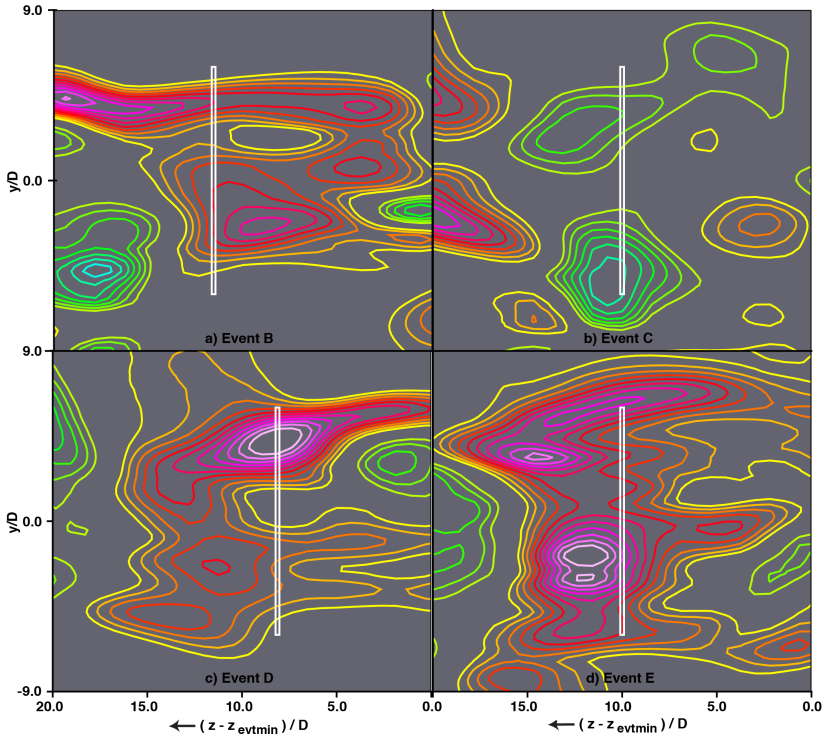

Fig. 7. Contours of Σ in an end-plane (y, z) at x/D = 37.5, a) Event B, b) Event C, c) Event D & d) Event E, Case IN.

3.2 Case NS

The behavior of the upper and lower DSLs in the intermediate wake region in Case NS is investigated in this subsection. Figure 8 shows contours of cross-stream velocity (*v*) as a function of time and z (in a (t, z) plane) at x/D = 75.0 (intermediate wake), y /D = 0.0. In terms of the plate length (the same in Cases IN & NS) the location x/D = 75.0 in Case NS is identical to the location x/D = 37.5 in Case IN (the plate thickness in Case IN is twice that of Case NS). Qualitatively, Fig. 8 is quite similar to Fig. 4. Instantaneous spanwise vorticity contours in a (x, y) plane corresponding to the banded regions (as in Fig. 3) showed a wake instability. In the interest of brevity, they are not included here.

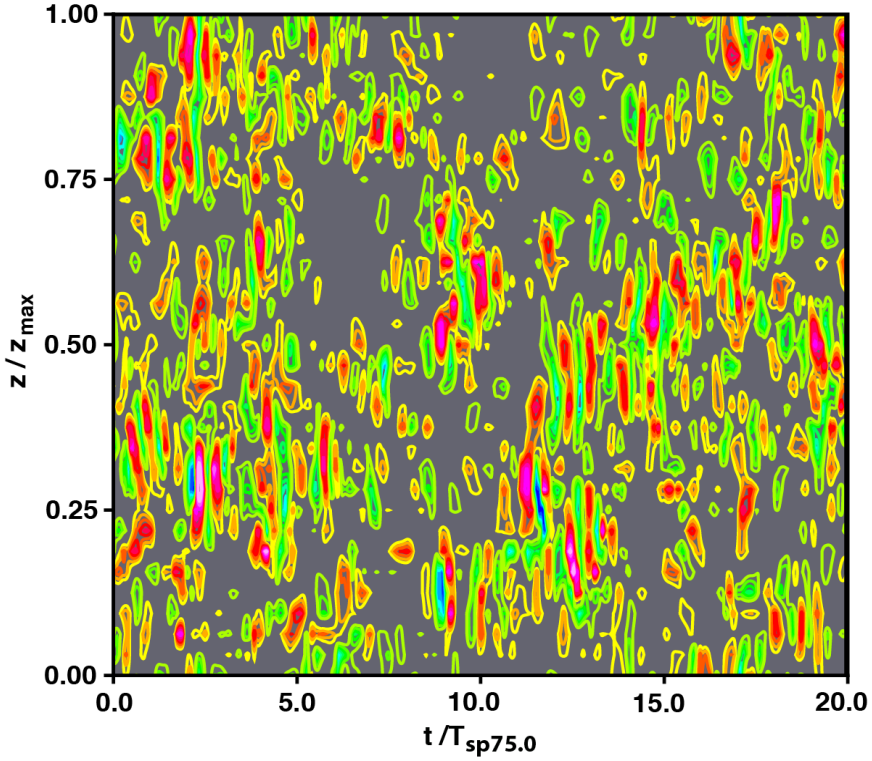

Fig. 8. Contours of *v* in a (t, z) plane at x/D = 75.0, y/D = 0.0, Case NS.

As in Case IN, the frequent occurrence of the intermediate-wake instability leads to the expectation of a broadband peak in the spectrum obtained for *v* at the location x/D = 75.0, y/D = 0.0. Figure 9 shows this spectrum along with the one obtained for Case IN at x/D = 37.5, y/D = 0.0. Frequency values are normalized with shedding frequency obtained in Case IN (as in Fig. 5). The spectrum obtained for Case NS has a broadband peak as well; the peak-related-frequency is about 92% of that obtained in Case IN. The spectrum obtained in Case NS is quite similar to that obtained in Case NS.

To summarize the findings of this section, both Cases IN and NS exhibit a wake instability in the intermediate wake. The instability is intermittent but occurs frequently and is sufficiently powerful to cause a broadband peak in the centerline *v* spectrum. The instability results in vortices near the wake centerline that are for the most part spanwise in orientation but may have streamwise and cross-stream components as well. Time periods in between instability events are characterized by relatively quiescent DSLs during which near-centerline vortices of the type encountered during an instability, are largely absent. The events observed showed both the DSLs being unstable, thus producing a string of vortices of alternating sign.

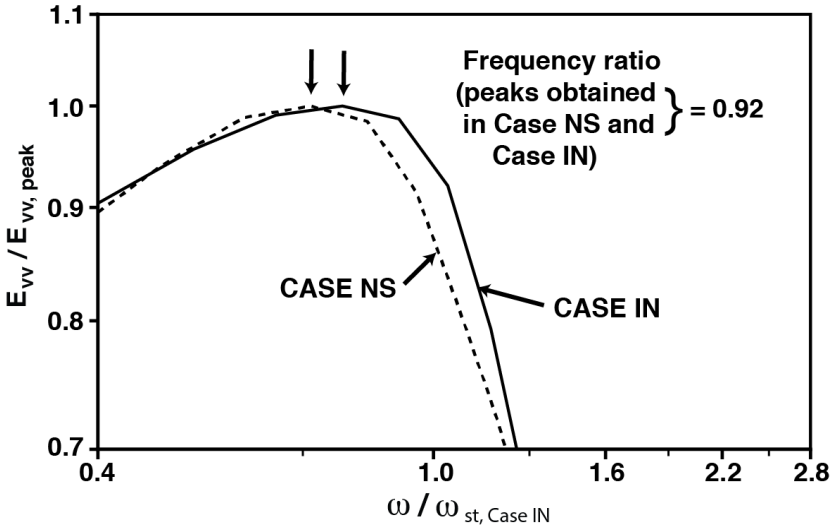

Fig. 9. Comparison of wake centerline *v* spectra obtained at x/D = 37.5 in Case IN and at x/D = 75.0 in Case NS.

4. VELOCITY-STATISTICS IN CASES IN & NS

Distributions of the turbulent normal intensities and shear stress are provided in this section. The distributions of the budget terms in the transport equation for the streamwise intensity are also included to provide a better understanding of the individual contributions to this component of intensity. The transport equations for the turbulent stresses (incompressible formulation, see for example Mansour et al. 1988) are provided in Eqs. 2 & 3:

$$\rho\frac{D\overline{u_i'u_j'}}{Dt} = P_{ij} + T_{ij} + \Pi_{ij} + D_{ij} - \varepsilon_{ij} \qquad (2)$$

where ρ is the density, and the terms in Eq. 2 are defined below;

$$\frac{D\overline{u_i'u_j'}}{Dt} = \frac{\partial\overline{u_i'u_j'}}{\partial t} + \overline{u_k}\frac{\partial\overline{u_i'u_j'}}{\partial x_k}$$

$$P_{ij} = -\rho\left\{\overline{u_j'u_k'}\frac{\partial\overline{u_i}}{\partial x_k} + \overline{u_i'u_k'}\frac{\partial\overline{u_j}}{\partial x_k}\right\} \qquad Production\ Rate$$

$$T_{ij} = -\rho\left\{\frac{\partial\overline{u_i'u_j'u_k'}}{\partial x_k}\right\} \qquad Turbulent\ transport\ rate$$

$$\Pi_{ij} = -\left\{\overline{u_j'\frac{\partial p'}{\partial x_i} + u_i'\frac{\partial p'}{\partial x_j}}\right\} \qquad Velocity\ pressure-gradient\ term$$

$$D_{ij} = \mu\nabla^2\overline{u_i'u_j'} \qquad Viscous\ diffusion\ rate$$

$$\varepsilon_{ij} = 2\mu\left\{\overline{\frac{\partial u_i'}{\partial x_k}\frac{\partial u_j'}{\partial x_k}}\right\} \qquad Dissipation\ rate \qquad (3)$$

In Eqs. 2 & 3, p is the pressure, u_i (i = 1, 2, 3) are the velocity components in the streamwise, cross-stream and spanwise directions (x_i), μ is the viscosity of the fluid and repeated indices denote summation.

Figures 10a and 10b show time-averaged distributions of the turbulent streamwise and cross-stream normal intensities and Fig. 10c the shear stress in the wake region for Case IN in the region 0.0 < x/D < 125.0, -25.0 < y/D < 25.0. The minimum and maximum values and the number of contours in each sub-plot of Fig. 10 are the same. The factor F in each subplot is the factor with which the associated quantity is multiplied so that the main features are clearly observed (this is the case in Figs. 12a – 12c as well). The centerline values of the normal intensities initially increase with increasing x/D. Interestingly, peak values in streamwise intensity profiles (the peak occurs away from the centerline) also increase with the increasing x/D. This is consistent with the findings of Hayakawa and Iida (1992). Instability-related vortices are potential contributors to the peaks observed in profiles of streamwise intensity. Appreciable peak values in shear stress profiles only develop past about x/D = 20.0 (off-centerline profile peaks), indicating that this phenomenon is related to the wake instability as well. The intensity and shear stress distributions obtained in Case NS are quite similar to those of Case IN.

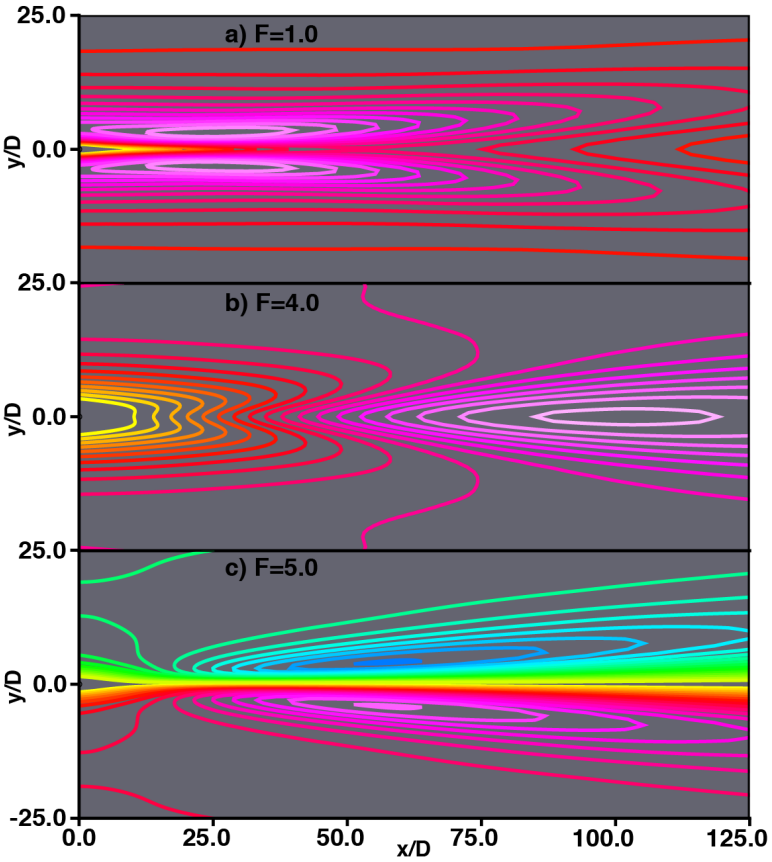

Fig. 10. Time-averaged distributions of turbulent a) streamwise & b) cross-stream intensities, and c) shear stress.

Figure 11 compares centerline normal intensities obtained in Cases IN and NS. Intensity values are normalized with the peak centerline value of streamwise intensity obtained in Case IN. The streamwise distance x is normalized with the plate thickness of Case IN (D_{IN}). Clearly, both the streamwise and cross-stream components of intensity obtained in the two cases are in close proximity; that is, the trailing edge diameter only has a minor effect on centerline intensity distributions (away from the near trailing edge region) when the plate thickness is small in relation to boundary layer thickness.

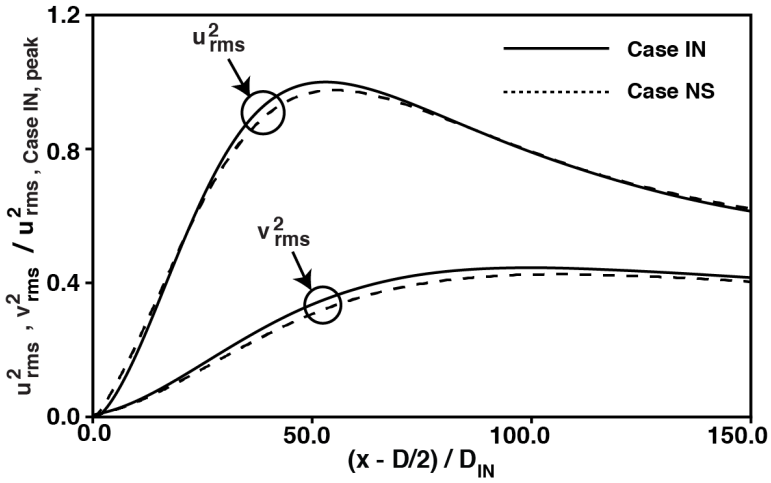

Fig. 11. Centerline normal intensity variation with x in Cases IN & NS.

Time-averaged distributions of the production, transport and diffusion terms (Eqs. 2 & 3) for the streamwise normal intensity are provided in Figs. 12a, 12b & 12c, respectively.

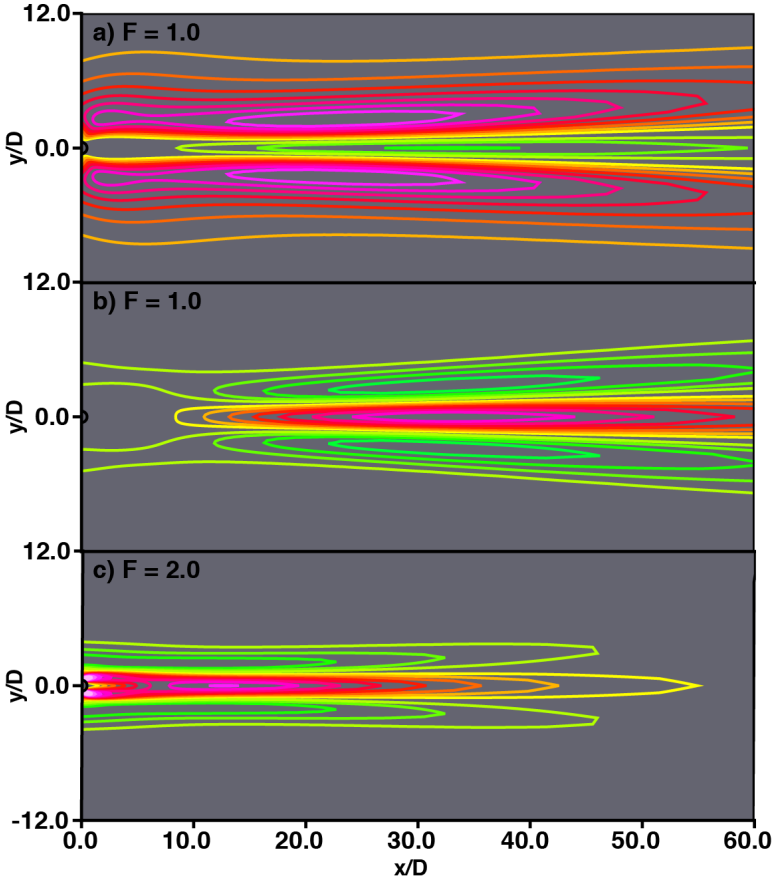

Fig. 12. Time-averaged distributions of a) production rate, b) transport rate and c) diffusion rate.

Interestingly, while the production term is certainly positive away from the centerline (it attains a peak value in the same general area where the streamwise intensity peaks in Fig. 10a), it is mostly negative along the

centerline in Fig. 12a. Thus, it does not explain increasing streamwise intensity with increasing x (Fig. 11, x/D < 53.5). However, the transport term shows transport from the intensity peaks located above and below the centerline towards the centerline. In addition, the diffusion term is appreciable and plays a similar role. Thus, the transport and diffusion processes run counter to production near the centerline and help to explain the observed increase in intensity for x/D < 53.5.

A more quantitative understanding of the contributions of all the budget terms in Eqs. 2 & 3 on the centerline streamwise intensity variation can be obtained from Fig. 13 where these terms are plotted as a function of x/D. The term R_{11} is the sum of all the budget terms. All the terms are normalized with the peak centerline value of R_{11}. The magnitude of R_{11} tapers off rapidly past its peak and turns negative at about x/D = 53.5 (the location beyond which the streamwise intensity decreases in Fig. 11). Clearly all the terms contribute appreciably to the overall budget with transport playing a dominant role. The instability related vortices are potential contributors to the importance of transport. In the interest of brevity, a similar discussion of the budget terms for the cross-stream intensity and shear stress are not provided here.

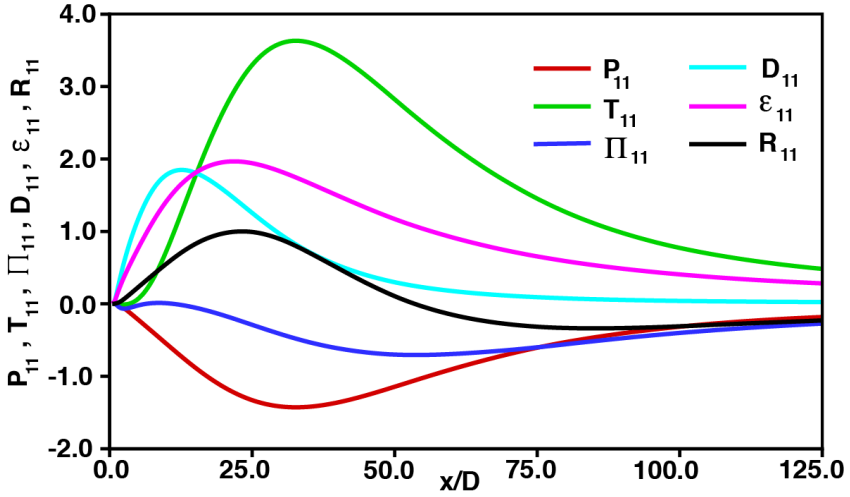

Fig. 13. Centerline variation of the budget terms (Eqs. 2 & 3), Case IN.

5. CONCLUDING REMARKS

The intermediate wakes of thin flat plates with circular trailing edges are investigated with direct numerical simulations (Cases IN and NS). The plate thickness in Case NS is half that of Case IN. The separating boundary layers are turbulent in both cases. The very near wake of these two cases, with a focus on the vortex shedding process, was explored in a recent article. Intermittent shedding was observed in Case IN. Case NS was an essentially non-shedding case. A third case (ST) with a sharp trailing edge was also investigated and found to exhibit an intermittent wake instability. The objectives of the present study are twofold. The first is to determine if the wake instability found in Case ST exists in Cases IN and NS as well. The second is to provide the distributions of the turbulent normal intensities and shear stress in the wake and to understand these distributions via the budget terms in the corresponding transport equations.

Both Cases IN and NS exhibit a wake instability in the intermediate wake. The instability is intermittent but occurs frequently and is sufficiently powerful to cause a broadband peak in the centerline *v* spectrum. The instability results in a string of vortices near the wake centerline that are for the most part spanwise in orientation but may have streamwise and cross-stream components as well. Time periods in between instability events are characterized by relatively quiescent DSLs during which near-centerline

vortices of the type encountered during an instability are largely absent. The events observed showed both the upper and lower DSLs being unstable, thus producing a string of vortices of alternating sign. A point of interest is that Case IN exhibits both intermittent shedding at the plate trailing edge (shed vortices are apparent only in the first few diameters) as well as the intermediate-wake instability.

The centerline values of the normal intensities initially increase with increasing x/D, reach a peak value, and then decrease. Interestingly, peak values in streamwise intensity *profiles* (the peak occurs away from the centerline) also increase with the increasing x/D (consistent with earlier experimental findings). Instability-related vortices are potential contributors to the peaks (off-centerline) observed in profiles of streamwise intensity. Appreciable peak values in shear stress profiles only develop past about x/D = 20.0 (off-centerline profile peaks), indicating that this phenomenon is related to the wake instability as well. The intensity and shear stress distributions obtained in Case NS are quite similar to those of Case IN.

Time-averaged distributions of the production, transport and diffusion terms for the streamwise normal intensity are provided. While the production term is positive away from the centerline, it is mostly negative along the centerline. Thus, it does not explain the initial increase in centerline streamwise intensity with x. However, the transport term shows transport from the intensity peaks located above and below the centerline towards the centerline. In addition, the diffusion term is appreciable and plays a similar role. Thus, the transport and diffusion processes run counter to production (negative) near the centerline and help to explain the observed increase in intensity for x/D < 53.5. The data show that all the budget terms contribute appreciably to the overall budget in the transport equation for streamwise normal intensity.

REFERENCES

ALBER, I. E. 1980 Turbulent wake of a thin, flat plate. *AIAA Journal*, Vol. 18 (9), 1044.

CHEVRAY, R. & KOVASZNAY, L. S. G. 1969 Turbulence measurements in the wake of a thin flat plate. *AIAA Journal*, Vol. 7, 1641.

HAYAKAWA, M. & Iida, S. –I. 1992 Behavior of turbulence in the near wake of a flat plate at low Reynolds number. *Physics of Fluids A*, Vol. 4 (10) 2282.

JEONG, J. & HUSSAIN, F. 1995 On the identification of a vortex. *Journal of Fluid Mechanics*, Vol. 285, 69.

KARLSSON, R. I. & JOHANSSON, T. G. 1988 LDV Measurements of higher-order moments of velocity fluctuations in a turbulent boundary layer. Laser Anemometry in Fluid Mechanics, Ladoan-Instituto Superior Tecnico, Portugal, 273.

KIM, J., MOIN, P. & MOSER, R. 1987 Turbulence statistics in fully developed channel flow at low Reynolds number. *Journal of Fluid Mechanics,* Vol. 177, 133.

MANSOUR, N. N., KIM, J. & MOIN, P. 1988 Reynolds-stress and dissipation-rate budgets in a turbulent channel flow. *Journal of Fluid Mechanics,* Vol. 194, 15.

ONG, L., WALLACE, J., & MOIN, P. 1995 The velocity and vorticity fields of the turbulent near wake of a circular cylinder. NASA TM -110513.

NAKAYAMA, A. & LIU, B. 1990 The turbulent near wake of a flat plate at low Reynolds number. *Journal of Fluid Mechanics*, Vol. 217, 93.

RAI, M. M. & MOIN, P. 1991 Direct simulations of turbulent flow using finite-difference schemes. *Journal of Computational Physics* Vol. 96 (1), 15.

RAI, M. M. 2010 A computational investigation of the instability of the detached shear layers in the wake of a circular cylinder. *Journal of Fluid Mechanics*, Vol. 659, 375.

RAI, M. M. 2013 Flow physics in the turbulent near wake of a flat plate. *Journal of Fluid Mechanics*, Vol. 724, 704.

RAI, M. M. 2014 Flow Phenomena in the very near wake of a flat plate with a circular trailing edge. *Journal of Fluid Mechanics*, Volume 756, 510.

RAI, M. M. 2015 Detached shear-layer instability and entrainment in the wake of a flat plate with turbulent separating boundary layers. *Journal of Fluid Mechanics*, Vol. 774, 5.

RAI, M. M. 2017 Changes in flat plate wake characteristics obtained with decreasing plate thickness. *International Journal of Heat and Fluid Flow*, Vol. 68, 13.

RAI, M. M. 2018a Vortex Shedding Characteristics of the Wake of a Thin Flat Plate with a Circular Trailing edge. *International Journal of Heat and Fluid Flow*, Vol. 72, 20.

RAI, M. M. 2018b Intermittency and Cessation of vortex shedding in the wake of a thin flat plate with a circular trailing edge. NASA TM-2018-219976.

RAMAPRIYAN, B. R., PATEL, V. C. & SASTRY, M. S. 1982 The symmetric turbulent wake of a flat plate. *AIAA Journal*, Vol. 20 (9), 1228.

THOMAS, F. O., & LIU, X. 2004 An experimental investigation of symmetric and asymmetric turbulent wake development in pressure gradient. *Physics of Fluids*, Vol. 16, (5), 1725.